Transient Free-Surface Flows: Fluid Advancing Through a Bed of Cylinders

The flow of a viscous liquid into a bed filled with a regular array of cylinders was observed experimentally and simulated numerically. Viscous forces were always dominant, as is expected to be the case in many actual resin transfer molding operations.

Excellent agreement on the shape of the free surface was found between experiment and simulation over the full experimental range. The work accordingly validates a very simple algorithm for representing the surface motion of a fluid at its contact line with a solid surface, and extends its use to surfaces with smaller radii of curvature than considered previously. Consequently, this algorithm is expected to be valid for fluid flow into any irregularly shaped empty domain and to be useful in molding operations in inferring the presence of voiding, and of molecular orientations and conformations adjacent to fibers or other solids.

R. A. Behrens, M. J. Crochet
C. D. Denson, A. B. Metzner
Department of Chemical Engineering and
Center for Composite Materials
University of Delaware
Newark, DE 19716

Introduction

We wish to describe in detail the motion of a liquid as it advances, with a free interface, through a loose array of cylinders placed perpendicularly to the advancing mass of liquid, as shown in Figures 1 and 2. In Figure 1 the flat liquid surface is shown advancing upward toward the array of cylinders but it has not yet reached or penetrated the array, and consequently the fluid interface is flat. Some time later, as seen in Figure 2 for one small portion of the overall flow domain, the liquid has advanced into the region between the cylinders and the advancing free liquid surface or flow front has adopted a smooth but complex geometry. It is this geometry that we wish to compute and to measure. Our motivation is as follows.

High-strength composites may be manufactured by placing a mat of long fibers into a mold, typically filling 20–50% of the mold volume, and then injecting a resin at the maximum possible flow rate to fill the remaining void space. The properties of the cooled and solidified composite structure resulting from such a resin transfer molding (RTM) process may be affected by the details of the flow front, including those areas initially bypassed, and by the orientation and conformation of the polymer molecules at their interfaces with the fibers. Consequently we wish to model the flow process in sufficient detail to be able to obtain the fluid velocities and deformation rates in this interfacial region. As a first step toward this goal we neglect the possibly viscoelastic nature of the polymeric fluid and the nonisothermal nature of the actual process.

In order to consider the interfacial region under conditions of actual interest we must also be able to predict the macroscopic flow rates of polymer within a mold. Substantial progress has been made in this area. Happel (1959) gave an early description of viscous flow relative to an array of cylinders using a cell model. Flow through porous media, using the traditional Ergun equation, has been described in detail by MacDonald and coworkers (1979). Kyan et al. (1970) extended the Ergun equation by including dissipation arising out of a slightly deforming fibrous mat. Gonzalez et al. (1981) and Gonzalez-Romero et al. (1985) employed Darcy's law to evaluate permeabilities of fiberglass mats used in the RTM process. These and others have shown that the macroscopic flow rates within a fiber mat may be characterized quite well for a particular mold geometry and chosen process conditions. Williams et al. (1974) tried to explain the pressure drop in terms of capillary forces for a free surface flowing lengthwise down a unidirectional bed of fibers. Simple capillary rise arguments first given by West (1911) and Washburn (1921) explain part of the observed pressure-throughput behavior. Gas bubbles trapped and held by surface and viscous forces were also observed. A surface-force-dominated flow, generated by immersing a single layer of woven fabric into a liquid, was studied by Miller and Clark (1978; also, Clark and Miller, 1978). The positive and negative pressure spikes observed were

Correspondence concerning this paper should be addressed to A. B. Metzner.
R. A. Behrens is currently with Chevron Oil Field Research Co., La Habra, CA 90631.
The permanent address of M. J. Crochet is Mecanique Appliquee, Universite Catholique de Louvain, Place du Levant, 2; B-1348 Louvain-la-Neuve, Belgium.

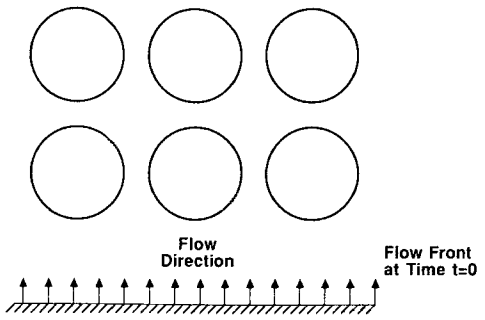

Figure 1. Geometry of flow process considered.

qualitatively explained by the high capillary forces. These works all dealt with the macroscopically observable variables of pressure and flow rate. We will proceed, therefore, with some confidence that local flow rates within a fiber mat may be characterized quite well for a particular mold geometry and chosen process conditions. Thus, it is now useful to consider the microscopic aspects of the flow at or near an interface.

For flows through ducts of simple geometry, recent analytic, numerical, and experimental results have been described by Beris (1987), Mavridis et al. (1986a,b), Behrens et al. (1987), and Coyle and coworkers (1987). We wish to extend their considerations to flows through the complex geometry of a model fiber mat. In RTM processes it may be of interest to know the details of the frontal fluid mechanics—just as it is helpful to study the fountain flow across the entire cavity thickness in injection molding operations. Additionally, it may be useful to identify any small areas between fibers not initially filled by the advancing front since these could lead to significant imperfections in a finished object. As a result of these considerations we will concentrate on the motion of the advancing frontal liquid.

The frontal geometry of the fluid in Figure 2 will be determined by the relative magnitudes of the viscous, gravitational, surface, and inertial forces. The small size of fibers and of the flow passages that are of interest in actual RTM processes, coupled with the limited resin velocities used to restrict fiber motion (so-called wash), restricts the Reynolds number level to the order of 10^{-1} to 10^{-3} (Behrens, 1983) and inertial effects can clearly be ignored. The ratios of gravitational to viscous forces, as measured by the Jeffreys number $\rho g L^2/\mu V$, are in the range

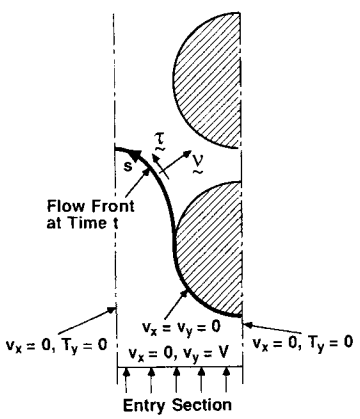

Figure 2. Evolution of flow process and description of boundary conditions.

of 10^{-4} to 10^{-2}, and hence gravitational contributions may likewise be omitted. Surface forces at the contact line between the advancing fluid and a cylindrical fiber require a somewhat more careful assessment. The review by Dussan (1979) provides a very good survey of the complexity of dynamic contact angles. It is important to note that viscous forces always tend to shift the contact angle away from its equilibrium value, as noted in drop spreading experiments by Welygan and Burns (1980) and by many students of the behavior of a sheet or tape plunging into a pool of liquid. In the latter area, the work of Inverarity (1969) is especially worthy of notice. Hoffman (1975, 1983) has presented a curve depicting the magnitude of this shift as a function of the capillary number $\mu V/\sigma$, for flow through a straight-walled tube. In our case the geometry may be much more complex but the contact angle will still be shifted toward a nonwetting angle. The ratio of surface to viscous forces in RTM processes, $\sigma \cos \theta/\mu V$, will usually be in the range of 10^{-2}–1.0 and only seldom greater than unity. Surface forces are therefore not expected to dominate viscous forces. Consequently we will neglect the former, but we will need to validate this assumption carefully when we turn to the experimental data.

In actual RTM processes the fluid flow will never be exactly perpendicular to an array of cylinders as depicted in Figure 1. However, fluid permeabilities tend to be far greater in the direction along a fiber axis and hence the geometry chosen represents that of the slowest and hence presumably rate-controlling flow. Additionally, the geometry of Figure 1 provides greater opportunities for gas entrapment by the advancing fluid in incompletely evacuated molds.

Quantitative Description of Flow Process

At time $t = 0$ a planar flow is set into motion with an upward velocity V, Figure 1. We wish to obtain the location of the free surface and the velocity field as the fluid invades the array of cylinders. For low values of the Reynolds number, the flow has the same symmetry as the array of cylinders; thus we may limit the flow domain to a channel half-width plus a cylinder radius, as shown in Figure 2 where we have represented the flow front at some arbitrary later time.

The equations of motion, when inertial and gravitational forces are neglected, are given by:

$$-\nabla p + \nabla \cdot \mathbf{T} = \mathbf{0} \tag{1}$$

wherein T, the extra-stress tensor, is given by:

$$\mathbf{T} = 2\mu\mathbf{d} \tag{2}$$

for a Newtonian fluid. We assume the fluid to be incompressible, that is:

$$\nabla \cdot v = 0 \tag{3}$$

The boundary conditions are indicated in detail in Figure 2. The entry section is located far enough from the cylinders so that we can impose there a uniform vertical velocity field. The usual boundary conditions of vanishing normal velocity and vanishing tangential force apply on the planes of symmetry, while both velocity components vanish on the wall of the cylinders. The no-slip boundary condition is enforced at the contact line as well as behind the fluid front. This is an important assumption, whose

validity has been well established in steady flows at the modest stress levels necessary, in RTM operations, to avoid fiber washing in the flow direction. Very complete descriptions of the high stress levels necessary for any slip to arise have recently been given by Ramamurthy (1987) and Young (1988).

In the presence of surface tension, the surface force f per unit area of the flow front is given by:

$$f = \sigma \frac{d\tau}{ds} \tag{4}$$

where σ is the surface tension coefficient, τ is the unit tangent to the flow front with the domain on its left, and s is the corresponding curvilinear coordinate.

It is obvious that the flow problem described above is impossible to solve analytically, and we must resort to numerical techniques.

The Numerical Method. The numerical algorithm developed for solving the flow problem may be organized in three parts:

1. Calculation of the velocity and pressure fields
2. Calculation of the moving flow front
3. A remeshing procedure for the expanding flow domain

The velocity and pressure fields are calculated for a set of discrete times t_n, at which the flow domain is covered by a mesh of finite elements. In our calculations, we have used a combination of isoparametric nine-node Lagrangian elements and six-node triangular elements. The velocity and the pressure fields are approximated in terms of nodal values V_i, P_i and their respective shape functions Ψ_i and ϕ_i, that is:

$$v = \sum_{i=1}^{M} V_i \Psi_i, \quad p = \sum_{i=1}^{N} P_i \phi_i \tag{5}$$

where M and N denote the number of velocity nodes and pressure nodes, respectively. The velocity and pressure representations are both continuous. The Ψ_i's and the ϕ_i are, respectively, biquadratic and bilinear functions on quadrilateral elements, and complete second-degree and first-degree polynomials on triangular elements.

At a fixed time t_n the nodal velocity and pressure components are calculated by means of the Galerkin formulation (Crochet et al., 1984). Let Ω_n denote the flow domain at time t_n; for every shape function Ψ_i and ϕ_i we require that:

$$\int_{\Omega_n} \Psi_i(-\nabla p + \nabla \cdot \boldsymbol{T})\, d\Omega = 0$$

$$\int_{\Omega_n} \Psi_i \nabla \cdot v\, d\Omega = 0 \tag{6}$$

The divergence theorem is applied to Eq. 6 in order to obtain the weak form of the equations of motion, that is:

$$\int_{\Omega_n} [\nabla \psi_i \cdot (-pI + \boldsymbol{T})]\, d\Omega = \int_{\partial\Omega_f} \psi_i f\, ds \tag{7}$$

where $\partial\Omega_f$ spans an element on the partial boundary corresponding to the free surface. A further integration by parts must be performed on the righthand side of Eq. 7, since, with our present isoparametric elements, the boundary curve is only C^0-continuous; in view of Eq. 4 we have:

$$\int_{\partial\Omega} \psi_i f\, ds = \int_{\partial\Omega} \psi_i \sigma \frac{d\tau}{ds}\, ds \tag{8a}$$

$$= -\int_{\partial\Omega} \frac{\partial \psi_i}{\partial s} \sigma\tau\, ds + [\psi_i \sigma\tau]_{S_1}^{S_2} \tag{8b}$$

where S_1, S_2 are the values of the curvilinear coordinate at both ends of the free surface element. Following Ruschak (1980), we perform an integration by parts so as to decrease the derivative from second order in Eq. 8a to first order. (Equation 8a is second order since $d\tau/ds$ contains second-order partial derivatives.) The first-order derivative is desirable because it requires only a first-order continuity within the elements.

Once the velocity and pressure fields have been calculated at time t_n, we need to calculate the new location of the moving flow front. The predictor-corrector method given by Gresho et al. (1980) and used for updating the free surface has been described in detail in our earlier paper (Behrens et al. 1987) and will just be briefly described here. The procedure is summarized in Figure 3. At time t_n we choose a time step Δt in such a way

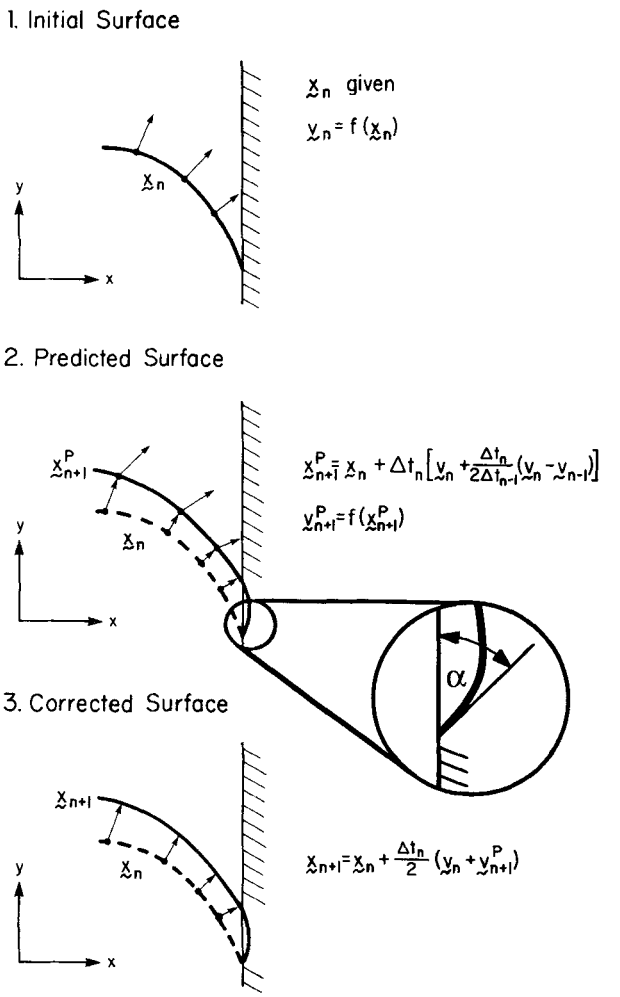

Figure 3. Portrayal of contact line movement with predictor-corrector method used for numerical calculations.

that none of the boundary nodes will cross the solid boundary within the time interval $[t_n, t_n + \Delta t]$. The provisional contact line is defined as the intersection of the isoparametric line passing through the updated nodes and the solid boundary. The predicted velocity field is recalculated on the updated finite element mesh, and the final location of the boundary is calculated on the basis of an average between the velocity field at time t_n and the predicted one. The transient contact angle and location of the contact point are natural results of the interplay between viscous and surface forces in the velocity calculation used in this procedure. Given sufficient distance in a uniform channel the contact angle will approach its steady state value, which is 180° for no-slip flows, as recently pointed out by Mavridis et al. (1988). The procedure used here avoids the *a priori* specification of the solid-liquid-vapor contact angle and as such it appears to represent an advance over other recent treatments of this topic. The procedure used accommodates both stationary and moving contact lines without special provisions by allowing the contact line only to move by a rolling motion. This rolling motion is proper for a no-slip boundary condition; it does not apply when surface forces dominate over viscous effects. The small loss of material near the contact line is minimized by means of a strict control on time step size that allows no more than one-third of the element surface outside of the boundary, so the angle α in Figure 3 always remains small. The amount of material lost is typically less than 0.01% of the volume swept by the time step. The drawing in Figure 3 greatly exaggerates, for visual purposes, the lost material. A delicate part of the numerical algorithm is to generate a new appropriate finite element mesh at each new time t_n. The procedure is easy for the predictor-corrector part of the algorithm, where it is sufficient to upgrade the coordinates of the free surface. However, the distortion of the flow domain during the filling process is so important that a global remeshing procedure must be implemented. The remeshing algorithm must

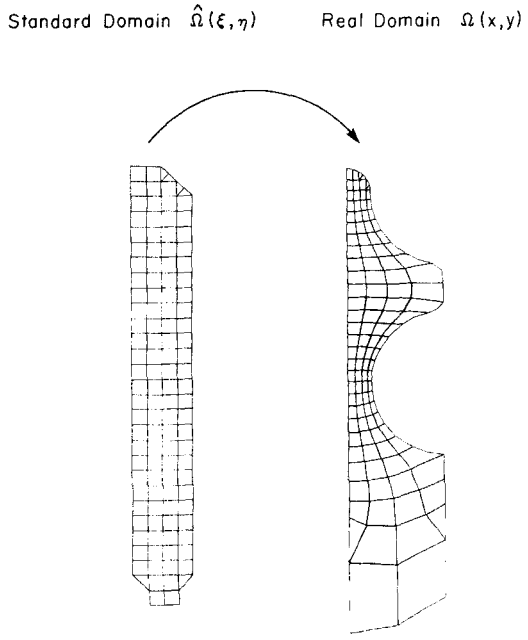

Figure 4. Automatic mesh generation transforms static mesh onto dynamic mesh.

Boundary points set by inverse weighted arc lengths give good mesh.

be able to generate elements that have both a proper shape and a proper size. We have used here a Laplacian technique in which a standard mesh is transformed onto an irregular domain, as first demonstrated by Winslow (1967) and further explained by Denayer (1980). Good reviews of grid generation problems have been provided by Thacker (1980) and Eisman (1985).

Let us consider in Figure 4 the flow domain at time t_n, which has a complicated shape once the fluid has penetrated the array of cylinders. We select at the outset a standard domain $\hat{\Omega}$ defined in terms of standard Cartesian coordinates ξ and η. The finite element topology in $\hat{\Omega}$ is fixed once and for all. At every time step, one imposes a correspondence between the boundary nodes of $\hat{\Omega}$ and those of $\hat{\Omega}$. The problem is to characterize the relationship:

$$x = x(\xi, \eta\,\cdot), \quad y = y(\xi, \eta\,\cdot) \tag{9}$$

between $\hat{\Omega}$ and Ω. The Laplacian procedure consists in imposing that x and y are harmonic functions, that is:

$$\frac{\partial^2 x}{\partial \xi^2} + \frac{\partial^2 x}{\partial \eta^2} = 0$$
$$\frac{\partial^2 y}{\partial \xi^2} + \frac{d^2 y}{\partial \eta^2} = 0 \tag{10}$$

Equations 10 are easily solved by means of a finite element discretization over $\hat{\Omega}$, that is:

$$x = \Sigma\, x_i \phi_i(\xi, \eta), \quad y = \Sigma\, y_i \phi_i(\xi, \eta) \tag{11}$$

and the usual Galerkin procedure, which is cheap and easy to apply on a standard mesh such as $\hat{\Omega}$ depicted in Figure 4.

The remaining difficulty is to set the proper values of the coordinates on the boundary of Ω. Such simple ideas as regular spacing along the boundary may lead to highly distorted finite elements, which would lead to severe discretization errors. A typical unacceptable finite element mesh is shown in Figure 5. Two specific techniques have been implemented in solving Eq. 10 to generate acceptable finite element meshes. Laplace's equation may be solved with either Dirichlet or Neumann boundary conditions. Referring again to Figure 4, we wish to impose the location of the nodes along the free surface and on the cylindrical walls (Dirichlet boundary condition) while we wish to generate element sides that are orthogonal to the plane of symmetry on the lefthand side of the domain in Figure 4. This is easily obtained by imposing the value of x along the plane of symmetry, while a Neumann boundary condition is used for y, that is

$$\frac{\partial y}{\partial \xi} = 0 \text{ on the plane of symmetry} \tag{12}$$

A proper spacing of the boundary nodes on the irregular walls is critical for generating an acceptable mesh. A specific "inverse weighted arc length" technique has been developed in which the distance between nodal points on the irregular boundary is inversely proportional to their distance to the plane of symmetry. The irregular arc length is integrated with a weighting function equal to the distance to the plane of symmetry and is then divided into nearly equal segments for the internodal spacings. Special provisions are made so that each segment of free surface

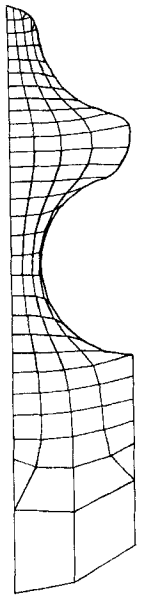

Figure 5. Mesh with boundary points set at equal arc lengths results in an inadequate finite element mesh.

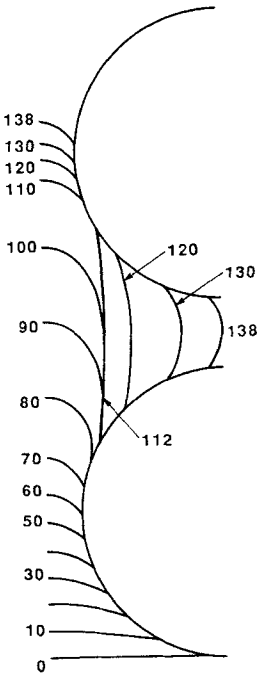

Figure 6. Calculated profiles of fluid moving upward through experimental geometry.

or fluid on a solid surface has at least one element assigned to it. The reallocation of boundary elements is made at each time step so that specific elements are never permanently devoted to any solid or free surface portion. As a result of the procedure, one may compare Figure 5, based on uniform spacing, and Figure 4 where the inverse weighted arc length method has been used.

Numerical results

Traces of the profiles of the advancing fluid in an evacuated mold are shown for one particular geometry in Figure 6. The ratio of the cylinder diameter to the separation of their centerlines is 0.798, giving an overall void fraction of 50%. The flow enters at the bottom with a perfectly flat profile at time step 0. Every tenth time step of the computation is shown. After 50 time steps the flow at the center of the void space (left side of the figure) has risen to about the level of the centerline of the first row of cylinders; the viscous drag at the surface of the cylinder has retarded the flow at the interface but, in fact, not at all greatly. In contrast after 80 time steps a tongue of fluid has begun to form as the fluid velocity at the center of the void space greatly exceeds that of the contact line movement. Since gravitational forces are negligible in comparison to viscous forces, this tongue is able to grow progressively (90 to 100 time steps) until, after 110 steps, it just reaches the second row of cylinders. If the mold were not evacuated, the shape of the profile at this time would determine the magnitude of the volume of air entrapped between the cylinders. This fluid contact with the second row of cylinders now provides additional viscous resistance to upward movement of the advancing fluid and it begins to move horizontally until, after 138 time steps, the horizontal tongue forming between the cylinders has reached the projection of the centerlines of the cylinders. This diversion from vertical to horizontal motion arises because the open cross-sectional area through which the flow occurs is seen to be larger in the horizontal than in the vertical direction after, say, 110 or 120 time steps.

Figure 7 shows this more clearly; there we observe the shapes of the streamlines after the 120th time step. In fact, as we can see from the numerical values of the stream function given on the streamlines, 90% of the flow is into the interstice between the cylinders and only 10% is moving upward into the second nip region. Clearly the fluid deformation rates at the interface with the cylinder will vary appreciably with angular position around the cylinder.

Figure 8 shows the corresponding pressure profiles after 120 time steps have been taken. The pressure units are nondimensionalized by the three parameters in the ratio $\mu V/B$, each of

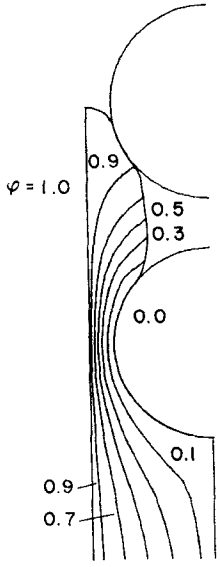

Figure 7. Calculated stream function contours at step 120.

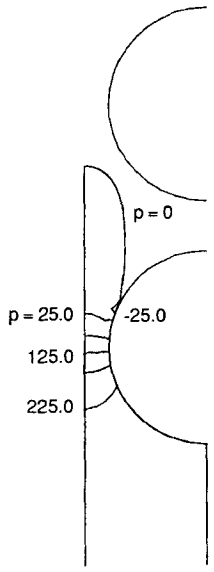

Figure 8. Calculated pressure contours at step 100.

which was set to unity in the simulation; the pressures thus reflect the units of these three parameters such as Pa from the combination of Pa · s, m/s, and m, respectively. The pressure at the bottom (one-half a minimum gap-width below the cylinder) is 280 units; at the level of the cylinder centerline it has decreased to 125, with most of the gradient occurring in this region of smallest cross-sectional area. The pressure gradient along the symmetry axis through the nip region is calculated to be approximately 40% higher than the pressure gradient for flow between parallel plates separated by the intercylinder distance; this is an important consideration in considering the deformation of fiber mats or fabrics by the flowing fluid. The pressure drop within the tongue extending to the next row of cylinders is only about 25 units since there is little fluid deformation in the upwardly advancing tongue of fluid. Again, large variations in the fluid stress level, hence of the molecular deformation and conformation in the case of a polymeric fluid, would be expected with position around each cylinder. The treatment of the transient contact line given here should be applicable to polymeric fluids qualitatively, although any rigorous transient flow computations involving memory fluids is considerably more difficult.

Experimental Method

The flow upward through a regular bank of cylinders (on a square pitch) of large size was studied, as shown on Figure 1. The cylinder diameters and lengths were 1.59 and 25.4 mm, respectively. The diameter was chosen for reasons of experimental convenience: large cylinders were chosen to enable detailed photographic observation of the motion of the contact line between the fluid and the cylinder as the flow progressed upward. The large 16:1 length to radius ratio was chosen in order to approximate a two-dimensional flow. The cylinder diameter is 79.8% of the cylinder center-to-center distance (50% solids loading). This spacing is referred to as $r/B = 0.798$, in which r refers to the cylinder radius and $2B$ is the center-to-center spacing of the cylinders.

In order to model the RTM process properly in the experiments the fluid chosen was sufficiently viscous to provide small Reynolds and Jeffreys numbers. At a velocity of 5 mm/s the pigmented polybutene oil used (Chevron 32), with a viscosity of 83 Pa · s at the experimental temperature of 22°C, gave Reynolds and Jeffreys numbers of 2×10^{-4} and 0.5, respectively. Viscous heating effects were neglected as the maximum adiabatic temperature rise of fluid was only 0.02°C. However, the intense lights used for the photography were found to cause major nonisothermal flow effects if left on continuously. Consequently they were only switched on intermittently for 1–2 s as needed. The flow was photographed with an H-16 Bolex 16 mm movie camera. A 100 mm telephoto lens was used with a 150 mm lens extension to give a large image on the film.

The flow channel was carefully machined from Plexiglas with tolerances typically within 0.05 mm. The cylinders were sections cut from a ground glass rod. The fluid flow was extremely sensitive to small asymmetries in the flow channel. The order or assembly of the channel could produce slight changes in the channel geometry that were not discernible through the camera in spite of the high magnification used, yet the changes could be large enough to cause major departures from the desired symmetric flow pattern. The channel had only one square pattern of cylinders in order to minimize the large pressure drop created by the combination of high viscosity and flow rate needed to negate the effects of gravity. The higher pressure drop that a second set of cylinders would have caused was unacceptable because it would have produced large stresses on the Plexiglas block, which would have altered the critical dimensions of the channel. Full details are available in the dissertation by Behrens (1983).

Experimental Results

Composite sketches of the interface for each movie frame were drawn for each of the experimental runs; one of these sketches appears in Figure 9. The entire sequence took less than 1 s and was recorded at 30 frames/s. The tracings are nearly symmetric about the centerline; the corresponding composite sketch for the numerical simulation in the same geometry was given in Figure 6, in which the interface corresponding to every tenth time step is shown. If the experimental flow in Figure 9 were a true two-dimensional flow, and if the numerical modeling were exact, Figures 6 and 9 would correspond exactly. Qualitatively they do appear to be very similar, the principal difference being an apparent broadening of the tongue that arises in the experiment because the fluid adheres not only to (long) cylindrical surfaces shown in Figures 6 and 9 but also to the end walls of the apparatus, which are also seen by the camera. A further comparison may be made between profile 16 of Figure 9 and profile 110 of Figure 6: these are profiles of the flow field just as it reaches the second row of cylinders. Integration of cross-sectional areas of these profiles shows they differ by only 3.5%, the experimental one being broader due to the apparatus end effects.

To quantify the agreement between the experiment and the numerical simulation, Figure 10 shows the axial and lateral extents (height and maximum width) of the fluid tongue as a function of time. The extents of the tongue are normalized by half of the center-to-center spacing between cylinders, B. The time is normalized with the flow rate and the maximum cross-sectional area for flow so that one unit of time would displace the front a unit distance with a flat interface in the absence of cylin-

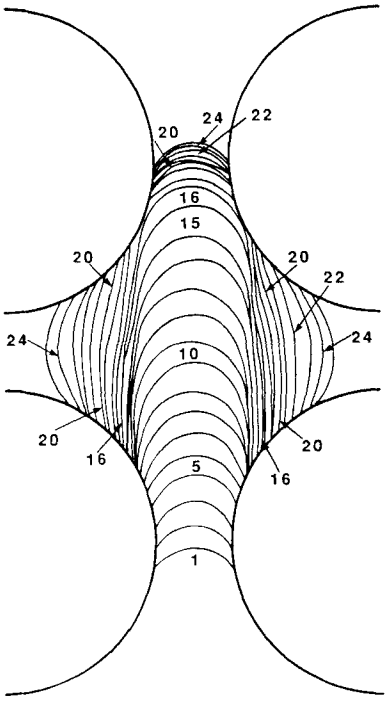

Figure 9. Experimental surface profiles advance through cylinders.
$r/B = 0.798$

ders. This normalization overcomes any minor inconstancies in both the camera speed and the flow rate.

The lateral extent curve starts at unity because the free surface extends across the entire gap. It quickly decreases as the fluid is squeezed into the nip. The lateral extent remains small while the tongue is in the interstice: the narrow tongue only occupies 34% of the flow channel at its widest point. However, the tongue swells quickly once it has contacted the next cylinders (at $t = 0.845$ in Figure 10). The change in slope of the lateral extent at this transition is not as noticeable for the experimental results as for the numerical calculation. This is because the broadening of the tongue occurred more gradually, due to end effects, as the tongue progressed through the nip. The axial extent, however, displays a marked change in slope both numerically and experimentally as the tongue contacts the next cylinder. The lower value of the slope near the end of the flow process

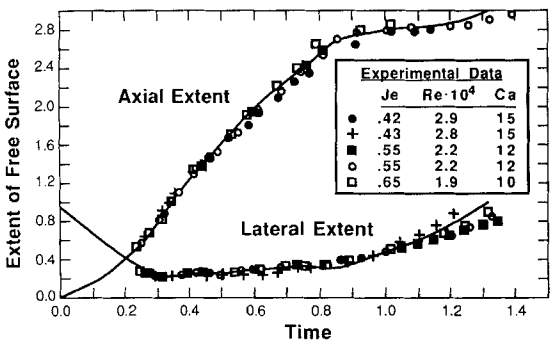

Figure 10. Calculated (curves) and experimental fluid front geometries.

($t > 0.85$) is due to the fluid preferentially squeezing laterally into the larger gap rather than proceeding upward into the narrow gap.

The agreement between the numerical simulation and all five sets of experimental data is seen to be excellent in Figure 10. The capillary number was always sufficiently great for surface tension to have no influence on the shape of the advancing liquid tongue. At the low values of the Reynolds numbers of the experiments one would expect no inertial effects and, indeed, none were present. The Jeffreys numbers of the experiments, extending to 0.65, were, however, large enough that one might have expected some influence of gravity to become evident. That this is clearly not the case for the data of Figure 10 suggests a broader range of validity for the numerical analysis than may have been anticipated.

Extension to Include Interfacial Tension Effects

The capillary numbers $\mu V/\sigma$ ranged from 10 to 15 for the experimental results shown in Figure 10 and so surface tension effects, ignored in the simulation, were clearly an order of magnitude smaller than viscous forces. However, capillary numbers as small as unity may be encountered in practical RTM processes and may be even smaller in some instances. Having established confidence in the finite element numerical simulation under the conditions used in our experiments, we may not extend the calculations to include conditions that may be encountered in practice but that are very difficult to attain in a laboratory simulation of the actual process.

Figure 11 shows the computed frontal profiles, just as the fluid tongue touches the second row of cylinders, for capillary numbers of 0.5 and 1.0 as well as the infinite value considered earlier. As expected, increasing the surface forces causes the more uniform rounding of the advancing tongue of liquid and the fluid appears to flow more rapidly into the interstice where

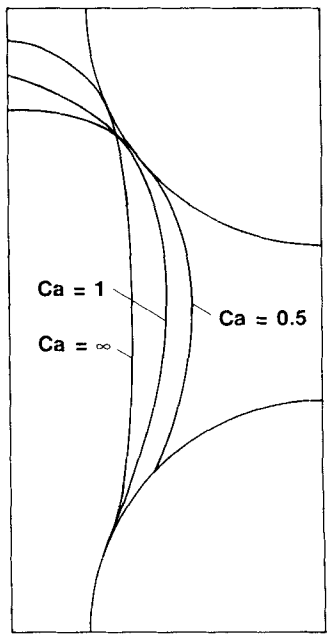

Figure 11. Effect of surface tension (capillary number) on geometry of advancing free surface of fluid.

Table 1. Unoccupied Cross-Sectional Area of the Mold During Flow

Capillary No. $\mu V/\sigma$	Static Contact Angle between Fluid and Fiber	Unoccupied Area %
∞	All angles	38
1	All angles	31
0.5	All angles	25
0	Nonwetting	19
0	Wetting	0

the resistance to flow is smallest. In this particular example the effect was exaggerated by reducing the fiber content of the mold from 50 to 44%. Table 1 summarizes these results in terms of the void fraction remaining in the fluid region of the mold when the resin first reaches the second layer of cylinders; this represents the maximum possible fraction of the air that could be trapped in an unevacuated mold. Also included, for comparison, are the limiting cases of infinite surface tension that might be encountered when injecting, instead of a polymeric fluid, a molten metal to form a metal-matrix composite product. The 19% void fraction is that which would arise when the large surface forces convert the advancing tongue of liquid into a perfectly circular geometry; the perfectly-wetting fluid advances from the top of one row of cylinders toward the next with a perfectly horizontal interface and so it always leaves a zero void. The finite void fractions in Table 1 would, of course, be greatly reduced in practice as the cylindrical surfaces would seldom be perfectly parallel as assumed in our calculations.

Conclusions

The complex flow patterns encountered in resin transfer molding processes have been simulated with the use of a finite element numerical method. Of critical importance in these calculations is the use of a very simple technique for predicting the motion of the contact line between the advancing fluid and the bounding surfaces, Figure 3. The computed flow patterns were shown to be in excellent agreement with the experimental measurements, thus validating not only the numerical method but also the handling of the difficult problem of the advancing fluid-solid contact line in these complex geometries. Consequently, we believe the same computational method may be applied with some confidence for the prediction of fluid motion for free-surface flows in general whenever the surface forces are dominated by the viscous forces in the range of $Ca \geq 0(1)$.

Acknowledgment

This work was supported by the industrial sponsors of the Center for Composite Materials.

Notation

B = half-gap width of flow channel, m
$\boldsymbol{d}$ = deformation rate tensor, 1/s
$\boldsymbol{f}$ = surface force vector, Pa
g = magnitude of gravitational force vector, N/m · s^2
$\boldsymbol{I}$ = identity tensor
L = length scale identified with cylinder diameter, m
p = isotropic pressure, Pa
P_i = nodal pressure at node i, Pa
r = Cylinder radius, m
s = arc length along irregular boundary, m
t = time, s
$\boldsymbol{T}$ = extra stress tensor, Pa
$\boldsymbol{v}$ = velocity vector, m/s
V = average velocity of cross section, m/s
$\boldsymbol{V}_i$ = nodal velocity vector at node i, m/s
x = x coordinate, m
y = y coordinate, m

Greek letters

η = y coordinate in standard domain
μ = shear viscosity, Pa · s
ξ = x coordinate in standard domain
ρ = fluid density, kg/m^3
σ = interfacial tension, N/m
ϕ = bilinear shape function
Ψ = biquadratic shape function
Ω = real domain
$\hat{\Omega}$ = standard domain
τ = unit vector tangent to flow front
ν = unit vector normal to flow front

Dimensionless groups

$Ca = \mu V/\sigma$
$Je = \rho g L^2/\mu V$
$Re = \rho V D/\mu$

Literature Cited

Behrens, R. A., "Transient Domain Free-Surface Flows and Their Applications to Mold Filling," Ph.D. Diss., Univ. Delaware (1983).

Behrens, R. A., M. J. Crochet, C. D. Denson, and A. B. Metzner, "Transient Free-Surface Flows: Motion of a Fluid Advancing in a Tube," *AIChE J.*, **33(7)** 1178 (July 1987).

Beris, A., "Fluid Elements Deformation behind an Advancing Flow Front," *J. Rheol.*, **31**, 121 (1987).

Clark, D. B., and B. Miller, "Liquid Transport through Fabrics; Wetting and Steady-State Flow. II: Fabric Wetting," *Text. Res. J.*, **48**, 256 (1978).

Coyle, D. J., J. W. Blake, and C. W. Macosko, "The Kinematics of Fountain Flow in Mold-Filling," *AIChE J.*, **33(7)**, 1168 (July 1987).

Crochet, M. J., A. R. Davies, and K. Walter, *Numerical Simulation of Non-Newtonian Flow*, Elsevier (1984).

Denayer, A., "Automatic Generation of Finite Element Meshes," *Comp. Struct.*, **9**, 359 (1980).

Dussan V., E. B., "On the Spreading of Liquids on Solid Surfaces: Static and Dynamic Contact Lines," *Ann. Rev. Fluid Mech.*, **11**, 371 (1979).

Eisman, P. R., "Grid Generation for Fluid Mechanics Computations," *Ann. Rev. Fluid Mech.*, **17**, 487 (1985).

Gonzalez, V. M., J. M. Castro, and C. W. Macosko, "Reaction Injection Mold Filling and Curing with *in situ* Fiberglass Mats," *World Cong. Chem. Eng.* Montreal (1981).

Gonzalez-Romero, V. M., and C. W. Macosko, "Adiabatic Filling through Packed Beds in Composite Reaction Injection Molding," *Poly. Proc. Eng.*, **3**, 173 (1985).

Gresho, P. M., R. L. Lee, S. T. Chan, and R. L. Sani, "A New Finite Element Technique for Boussinesq Fluids," *3rd Int. Conf. Finite Elements in Flow Problems*, Banff, Alberta, Canada (1980).

Happel, J., "Viscous Flow Relative to Arrays of Cylinders," *AIChE J.*, **5(2)**, 174 (June 1959).

Hoffman, R. L., "A Study of the Advancing Interface. I: Interface Shape in Liquid-Gas Systems," *J. Colloid Interf. Sci.*, **50**, 228 (1975).

———, "A Study of the Advancing Interface. II: Theoretical Prediction of the Dynamic Contact Angle in Liquid-Gas Systems," *J. Colloid Interf. Sci.*, **94**, 470 (1983).

Inverarity, G., "Dynamic Wetting of Glass Fibre and Polymer Fibre," *Br. Polym. J.*, **1**, 245 (1969).

Kyan, C. P., D. T. Wasan, and R. C. Kinter, "Flow of Single-Phase

Fluids through Fibrous Beds," *Int. Eng. Chem. Fundam.*, **9**, 596 (1970).
MacDonald, I. F., M. S. El-Sayed, K. Mow, and F. A. Dullien, "Flow through Porous Media—The Ergun Equation Revisted," *Ind. Eng. Chem. Fundam.*, **18**, 199 (1979).
Mavridis, H., A. N. Hrymak and J. Vlachopoulos, "Deformation and Orientation of Fluid Elements Behind an Advancing Flow Front," *J. Rheol.* **30**, 555 (1986a).
———, "Finite-Element Simulation of Fountain Flow in Injection Molding," *Polym. Eng. Sci.*, **26**, 449 (1986b).
———, "Transient Free-Surface Flows in Injection Mold Filling," *AIChE J.*, **34(3)**, 403 (March 1988).
Miller, B. and D. B. Clark, "Liquid Transport through Fabrics; Wetting and Steady-State Flow. I: A New Experimental Approach," *Text. Res. J.*, **48**, 150 (1978).
Ramamurthy, A. V., "Wall Slip in Viscous Fluids and Influence of Materials of Construction," *J. Rheol.*, **36**, 337 (1986).
Ruschak, K. J., "A Method for Incorporating Free Boundaries with Surface Tension in Finite Element Fluid-Flow Simulators," *Int. J. Num. Meth. Eng.*, **15**, 639 (1980).
Thacker, W. C. "A Brief Review of Techniques for Generating Irregular Computational Grids," *Int. J. Num. Meth. Eng.*, **15**, 1335 (1980).
Washburn, E. W. "The Dynamics of Capillary Flow," *Phys. Rev.*, **18**, 273 (1921).
Welygan, D. G., and C. M. Burns, "Dynamic Contact Angles of Viscous Fluids," *J. Adhesion*, **11**, 41 (1980).
West, G. D. "On the Resistance to the Motion of a Thread of Mercury in a Glass Tube," *Proc. Roy. Soc. London, Ser. A*, **86**, 20 (1911).
Williams, J. G., C. E. M. Morris, and B. C. Ennis, "Liquid Flow through Aligned Fiber Beds," *Poly. Eng. and Sci.*, **14**, 413 (1974).
Winslow, A. M. "Numerical Solution of the Quasilinear Poisson Equation in a Nonuniform Triangle Mesh," *J. Comp. Phys.*, **2**, 149 (1967).
Young, Albert, "Studies of Adhesion and Slip of Viscous Fluids and Gels at Solid Surfaces," Ph.D. Diss., Univ. Delaware (1988).

Manuscript received Oct. 12, 1987, and revision received July 11, 1988.